Proceedings of the ASME 2017 Pressure Vessels and Piping Conference
PVP2017
July 16-20, 2017, Waikoloa, Hawaii, United States

PVP2017-65471

IMPULSIVELY-GENERATED PRESSURE TRANSIENTS AND STRAINS IN A CYLINDRICAL FLUID-FILLED TUBE TERMINATED BY A CONVERGING SECTION

Jean-Christophe Veilleux and Joseph E. Shepherd
Graduate Aerospace Laboratories
California Institute of Technology
Pasadena, California 91106
Email: jc.veilleux@caltech.edu

ABSTRACT

The syringe in a subcutaneous autoinjector may be subjected to internal pressure transients due to the normal operation of the injection mechanism. These transients are similar to transients in fluid-filled pipelines observed during water hammer events. In this paper, the effect of an air gap in the syringe and a converging section are studied experimentally and numerically in a model system which consists of a fluid-filled metal tube that is impulsively loaded with a projectile to simulate the action of the autoinjector mechanism operation.

The air between the buffer and the water results in a complex interaction between the projectile and the buffer. Also, there are tension waves inside the tube due to the presence of a free surface, and this causes distributed cavitation which, in turn, gives rise to steepening of the pressure waves. The converging section can amplify the pressure waves if the wave front is sharp. Pressures as high as 50 MPa have been measured at the apex of the cone with impact velocities of 5.5 m/s.

INTRODUCTION

Autoinjectors are now ubiquitous in the pharmaceutical industry. These devices are both used with drugs to be administered in case of emergency (e.g., Epinephrine), and with drugs to be administered on a frequent basis (e.g., Alprostadil, Byetta, Enbrel). The popularity of autoinjectors is in part due to the compactness and the ease of use of the devices [1,2] and, more importantly, to a clear trend toward drugs that cannot be administered orally [3,4]. (For more details on autoinjectors see [3–5].)

Although the specific design of each autoinjector may differ, in most if not all of the devices currently available on the market, the mechanism is spring actuated [3]. Activation of the pen results in mechanical impacts between the moving components of the autoinjector mechanism. This can be an issue when very viscous drugs are to be injected since the large spring forces needed can result in failure of the device [6].

The filling process of the syringe typically results in an air bubble within the syringe. In the vertical orientation considered in this paper, the air bubble is located between the stopper and the drug solution.

The pressure transients inside the syringe have been experimentally measured (not reported in this paper). The results suggest the transients are similar to those observed in fluid-filled pipelines during water hammer events [7–9]. Inaba and Shepherd [10, 11] examined pressure transients which are closely related to the present work.

There are three main differences between the previous studies and the syringe situation: 1) the mechanism of initiating the transient; 2) the air gap; 3) the converging section. The aim of this paper is to investigate and explain the effect of these features on measured pressure and strains. This is achieved through experimental measurements and numerical simulations on a simplified setup six times larger than a typical syringe and constructed of metal rather than glass. It should be noted that the syringe model is static in this work; the effect of the translational motion is important but is not discussed in this paper.

The paper is organized as follows. First, the experimental setup is described. Second, the numerical methodology is pre-

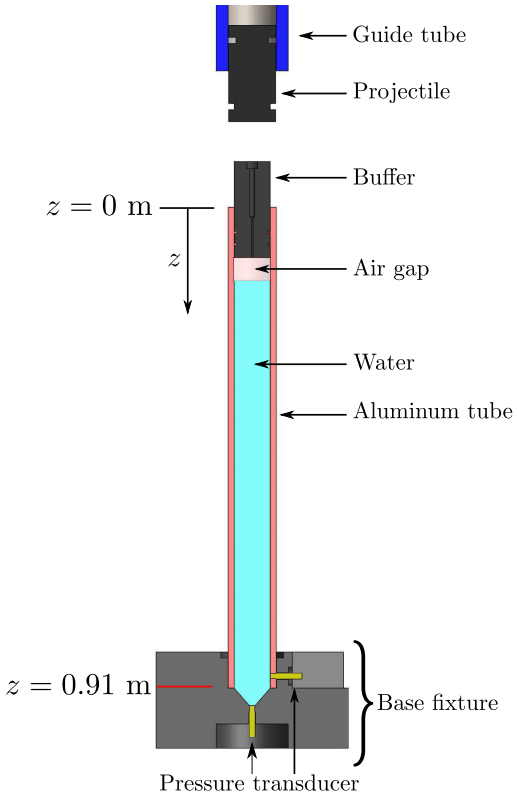

FIGURE 1: SCHEMATIC OF THE EXPERIMENTAL SETUP.

sented. Third, some results are shown for four cases which highlight the effect of an air gap and a converging section. Fourth and lastly, the findings are summarized in the conclusion.

EXPERIMENTAL SETUP

A schematic of the experimental setup is shown in Fig. 1. Note that the z-axis, or longitudinal axis, is defined downward positive, and all distances are relative to the top end of the tube. The experimental apparatus consists of three main components: the guide tube, the projectile, and the test specimen.

The guide tube has an inner diameter of 50.8 mm and a length of approximately 2.1 m (it is only partially shown in Fig. 1). The purpose of this tube is to guide the projectile while it is vertically accelerated to velocities up to 6.4 m/s using gravity alone. The projectile consists of a 0.5 kg aluminum cylinder which can slide freely within the guide tube.

The test specimen consists of an aluminum tube with a length of 0.91 m, an outer diameter of 50.8 mm and an inner diameter of 38.1 mm. The thick aluminum tube is filled with water, and it is pressed into a cylindrical base fixture which is bolted to heavy plates resting on the ground (not shown). Securing the aluminum tube into the base fixture was achieved using a shrink fit. The overall mass of the test specimen, including the

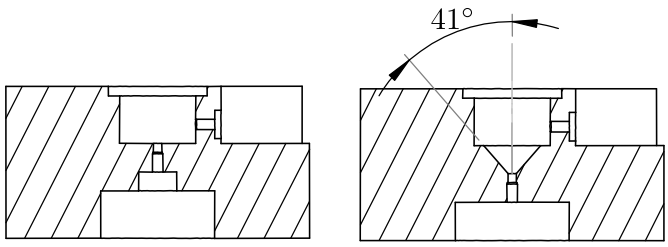

(a) WITHOUT A CONE (b) WITH A CONE

FIGURE 2: SCHEMATIC OF THE BASE FIXTURES.

TABLE 1: AXIAL LOCATION OF THE PRESSURE TRANSDUCERS.

Transducer	Without the cone	With the cone
P1	895 mm	895 mm
P2	910 mm	927 mm

base fixture and the plates, is over 50 kg.

Two geometries, which are shown in Fig. 2, have been tested. In the first geometry (Fig. 2a) the bottom of the aluminum tube is sealed with a flat end perpendicular to the longitudinal axis z. In the second geometry (Fig. 2b), the aluminum tube is sealed with a conical section similar to that of a syringe. The half-angle of the cone is 41°. In both geometries there are two ports for mounting pressure transducers.

The two pressure transducers mounted into the base fixture are also shown in Fig. 1. The exact locations of the transducers are indicated in Tab. 1. For the base fixture which has a conical section, one transducer is located above the converging section and the other one is positioned at the apex of the conical section.

The test specimen is sealed at its top end using a 104 mm long polycarbonate buffer. There are two O-rings between the buffer and the aluminum tube for proper sealing. There is a small hole along the longitudinal axis of the buffer which is closed using a socket screw before an experiment. This opening allows for the introduction of an air gap of controlled size between the bottom end of the buffer and the water contained in the tube. For all cases reported in this paper, the bottom end of the buffer is located at $z = (51 - d_0)$ mm, where d_0 is the initial air gap size.

In addition to the two pressure sensors (113A23 from PCB) there are 14 strain gauges to measure the hoop and axial strains at 7 axial locations on the outer wall of the aluminum tube. The strain gauges are a combination of CEA-06-125UN-350/P2 from

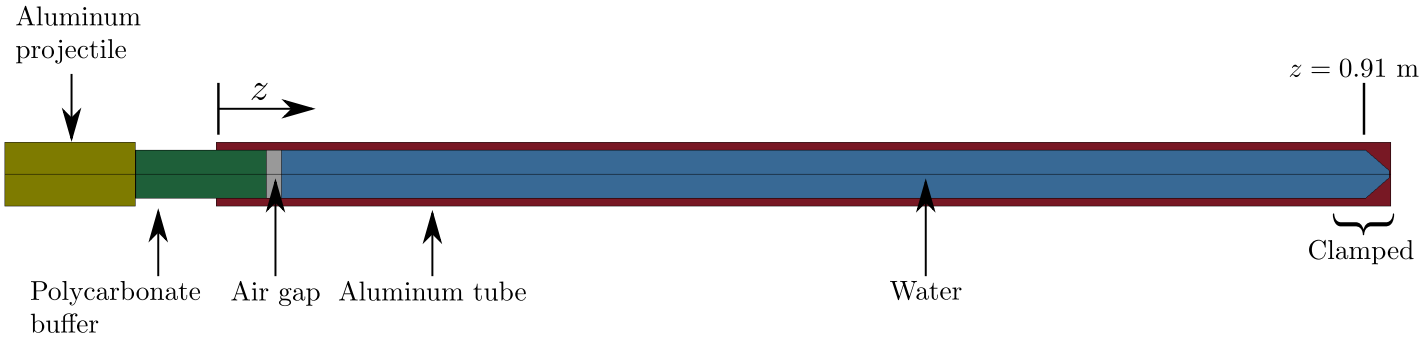

FIGURE 3: LS-DYNA MODEL FOR THE TEST SPECIMEN WITH A CONVERGING SECTION.

TABLE 2: AXIAL LOCATION OF THE STRAIN GAUGES.

Station	S1	S2	S3	S4	S5	S6	S7
z (mm)	127	254	381	508	635	762	857

Vishay and K-LY4-3-05-350-3-2 from HBM. The location of each gauge is indicated in Tab. 2.

A high-speed video camera (Vision Research Phantom V7.0G) is used to visualize the contact between the projectile and the buffer, making it possible to track the projectile and the buffer to study their interaction and to measure the impact velocity.

The analogy between the test setup and an actual autoinjector is as follows: the projectile corresponds to the spring actuated plunger rod, the buffer corresponds to the stopper, the aluminum tube corresponds to the glass syringe and the water corresponds to the drug solution.

Numerical Simulation

The numerical simulations have been performed using LS-DYNA [12], a general-purpose finite element code. LS-DYNA has the capability of handling fluid-structure interaction using some built-in features.

The geometry of the LS-DYNA model is shown in Fig. 3. The model is 2D axysimmetric and the mesh is constructed using Lagrangian shell elements. All components are meshed using a structured grid except for the conical section. The elements are approximately 0.5 mm x 0.5 mm in size unless otherwise indicated, and this yields a total of ≈110,000 elements. The time step Δt is chosen by the solver using the characteristic length of the elements L and the sound speed a of the material: $\Delta t = \omega L/a$; ω is the Courant number and a value of 0.5 was used in all calculations.

The projectile, buffer, air gap, water and wall are all modeled as separate material regions or parts. The base fixture is not modeled and is approximately taken into account through a boundary condition; the nodes of the wall which would be in contact with the base fixture are all rigidly clamped. The elements forming the air gap are also constrained to avoid getting a highly distorted mesh; they can only deform axially.

The nodes at the buffer-air gap interface are shared by the two components. The same is true about the nodes at the air gap-water interface. For the cases where no air gap is present, the nodes at the buffer-water interface are shared by both parts. By sharing the nodes between two parts no contact model is needed.

At the projectile-buffer interface and at the water-wall interface, the LS-DYNA built-in surface-to-surface contact model is used [12]. This contact model can only account for compression between the two surfaces; tensile forces are not transmitted between the two surfaces such that the cavitation inception pressure corresponds to zero absolute pressure. This assumption is appropriate as long as there are a large number of relatively large nuclei such that surface tension effects are small. Whenever the liquid is under tension, there is a loss of contact between the water and the wall; some voids start forming. The growth and the collapse of those voids locally mimic the effect of the vapor bubbles during cavitation.

A linear-elastic constitutive model is used for all solid parts. A Mie-Grüneisen equation of state (see [13] for a brief description) is used for the water. The gas in the air gap is an isentropically compressed perfect gas (i.e., P/ρ^{γ} = constant)[1].

Initially, all components are at rest except for the projectile which is traveling at the impact velocity V_0. The projectile and the buffer are initially a small distance apart (0.1 mm). Gravity is not accounted for in the simulations. It was verified that further refinement of the grid and the time step by a factor of 4 does not affect the results significantly.

[1] Aluminum: ρ = 2712 kg/m^3, E = 69.6 GPa, ν = 0.33. Polycarbonate: ρ = 1200 kg/m^3, E = 2.6 GPa, ν = 0.37. Water: ρ_0 = 1000 kg/m^3, a = 1500 m/s, S_1 = 0, S_2 = 0, S_3 = 0,γ_0 = 0. Air: γ = 1.4.

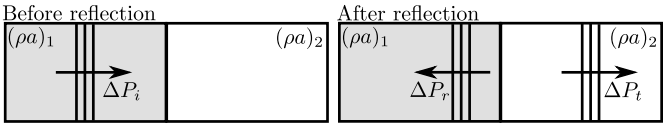

FIGURE 4: REFLECTION OF PRESSURE WAVES.

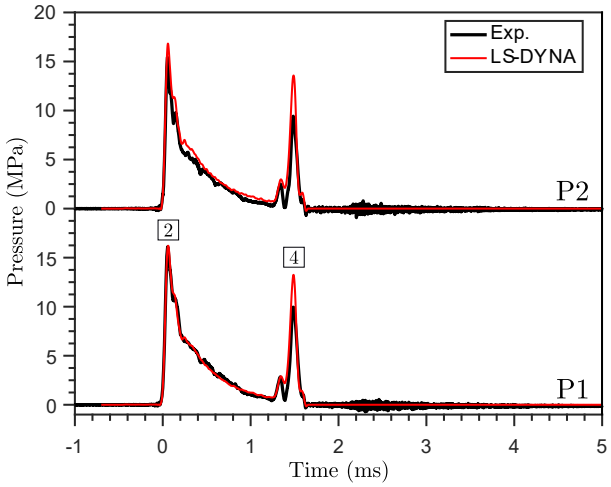

FIGURE 5: PRESSURE AT THE BOTTOM END (CASE 1).

RESULTS

Four cases are reported in this paper to illustrate the effect of an air gap and a converging section. In all cases, the impact velocity V_0 is approximately 5.5 m/s:

Case 1: no converging section, no air gap;
Case 2: no converging section, 3.5 mm air gap;
Case 3: no converging section, 12 mm air gap;
Case 4: with a converging section, 12 mm air gap.

Case 1

The first case is the simplest configuration with no air gap and no converging section. The water column is pressurized through a direct contact between the buffer and the liquid; the liquid at the interface is forced to move with the buffer.

This configuration was examined previously by Inaba and Shepherd [10,11] but without the base section used in the present study. Another difference is that Inaba and Shepherd used a clear, polycarbonate tube instead of an aluminum tube. As a result, the coupling between the liquid and the structure was substantially more important than in the present study. Despite the differences, the wave dynamics described in detail by Inaba and Shepherd are essentially the same as in the present study.

Because there are many reverberations of the stress waves

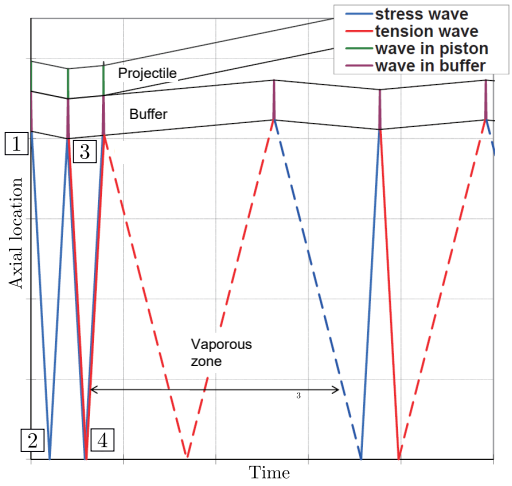

FIGURE 6: WAVE DYNAMICS IN THE TEST SETUP (ADAPTED FROM [10] WITH PERMISSION).

within the projectile and the buffer during the slowing of the buffer, the projectile and buffer can be treated as rigid bodies. The transit time of the stress waves is 36 μs in the projectile and 44 μs in the buffer; this is short compared to the rise time of the pressure. The idea that the motion of the projectile and the buffer is governed by rigid body mechanics has been validated through numerical simulations; making the buffer and the projectile rigid does not change the results other than producing a small increase of the peak pressures. This is of course a simplifying assumption, see [14] for a more detailed treatment of the wave dynamics in the projectile and buffer.

The maximum pressure in the liquid below the buffer can be estimated using acoustic theory [15]. Assuming the initial velocity of the buffer is the impact velocity V_0, $P_{max} \approx \rho a V_0$ and this yields a value of 8.3 MPa. As discussed in [11], we expect this pressure increase to be followed by an exponential decay since the projectile begins slowing down immediately after impact, thus creating expansion waves which follow the initial compression wave.

Because the pressure transducers P1 and P2 are located very close to the bottom wall where the wave will reflect, the measured peak pressure will be larger than 8.3 MPa. When the wave reaches the bottom wall, it will be partly transmitted through the base fixture and partly reflected into the water. Quantitatively, the reflected vs transmitted part of the wave is determined by the acoustic impedances (ρa) of the materials at the interface (see Fig. 4):

$$\Delta P_r = \left[\frac{(\rho a)_2 - (\rho a)_1}{(\rho a)_2 + (\rho a)_1}\right] \Delta P_i \qquad (1)$$

For the present experiment, medium 1 is water and medium 2

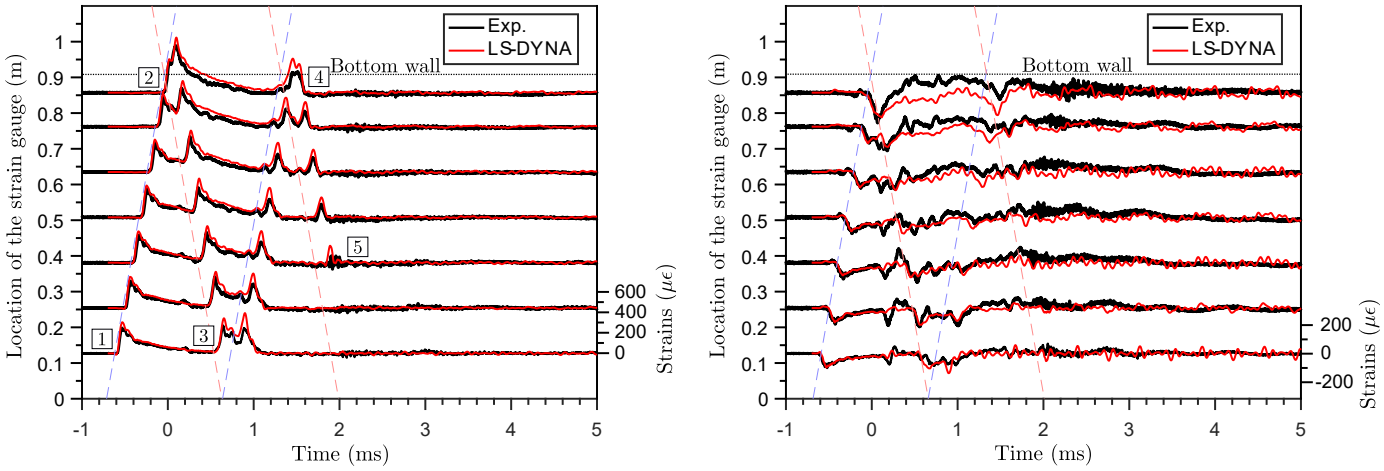

(a) HOOP STRAINS

(b) AXIAL STRAINS

FIGURE 7: HOOP AND AXIAL STRAINS (CASE 1).

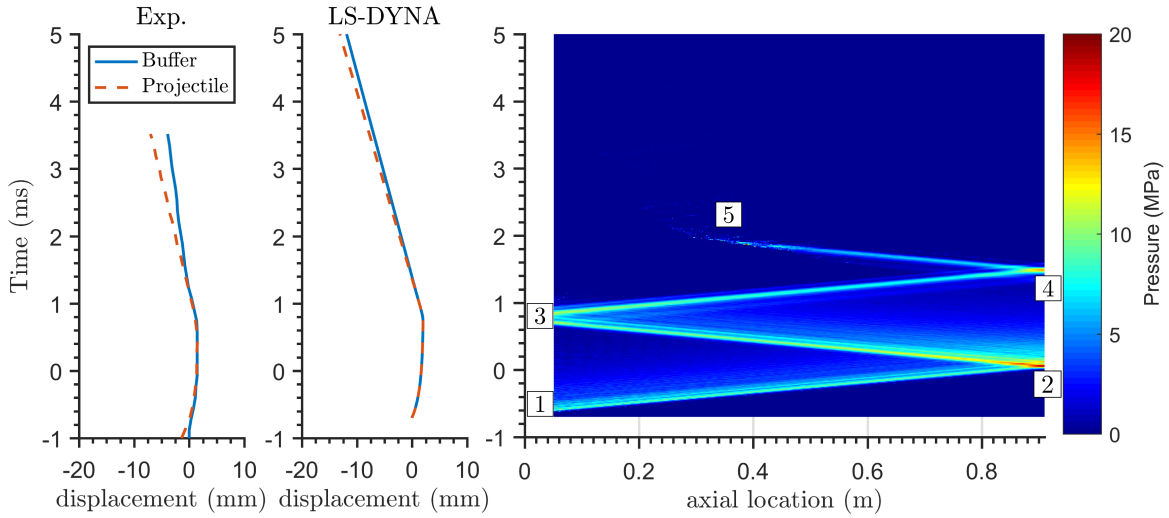

FIGURE 8: MOTION OF THE BUFFER AND THE PROJECTILE WITH A SPACE-TIME PRESSURE PLOT (CASE 1).

is aluminum: $\Delta P_r \approx 0.82\Delta P_i$. When the incident wave reflects at the wall, the pressure there is the sum of the incident and the reflected waves, that is 1.82 ΔP_i in the present case or $\approx$ 15 MPa.

Pressures P1 and P2 are shown in Fig. 5. Both P1 and P2 are very close in trend and magnitude; this is because there is no converging section and both pressure transducers are located only 50 mm apart. Also, the pressures from LS-DYNA are in good agreement with the experiment. The peak pressure is 16.0 MPa, which is very close to the estimate of 15 MPa obtained using acoustic theory. The first pressure wave is followed by a second wave of smaller amplitude (reaching the bottom at $\sim$ 1.4 ms), and this is immediately followed by cavitation. This is explained using Fig 6.

Upon impact of the projectile on the buffer (event 1), a stress (pressure) wave is produced in the liquid. This wave travels down the tube, partially reflects off the bottom wall (event 2) and then travels upward. After one round trip in the tube, the stress wave partially reflects on the buffer (event 3). The reflection of the wave on the buffer produces a second stress wave which later reaches the bottom of the tube (event 4). The reflection of the stress wave on the buffer (event 3) also initiates an upward motion of the buffer. This produces a tension wave which immediately follows the second stress wave. The tension wave produces distributed cavitation in the water column.

The hoop (ε_θ) and axial (ε_z) strains from the experiment and the simulations are shown in Fig. 7. The bottommost trace corresponds to location S1, and the topmost trace corresponds to location S7 as summarized in Tab. 2. The scale for the strains is shown to the right of the plot.

The oblique lines shown in Fig. 7 have a slope which corresponds to the Korteweg speed c. The Korteweg speed is the expected velocity of the pressure waves in the liquid for the fluid-structure coupled problem. It can be evaluated as follows:

$$c = \frac{a}{\sqrt{1+\beta}}\,, \tag{2}$$

where a is the sound speed in water, and $\beta = KD/(Eh)$ is the FSI coupling parameter with K the bulk modulus of water, D the average of the inner and outer diameter of the aluminum tube, E the Young's modulus of the tube, and h the thickness of the tube wall [11]. In the present case, $c = 1350$ m/s. Both liquid pressure waves and strains appear to propagate with the Korteweg speed.

Returning to Fig. 7, the agreement between the experiment and the simulations is good, especially for the hoop strains. The axial strains predicted by LS-DYNA close to the bottom of the test specimen are not as close to the experiment, and this could be due to the large sensitivity of the axial strains to the boundary conditions. It must be recalled that the base fixture and the plates to which it is bolted are not modeled in detail but the tube end is treated as fixed in space. On the contrary, the boundary conditions applied on the top end of the tube are modeled properly allowing motion in both radial and axial directions. There, the agreement between the experiment and the simulation is much better for axial strains.

We introduce in Fig. 8 a space-time plot of the pressure along with the motion of the projectile and the buffer. The measured and simulated motions of the projectile and buffer are in good agreement up to 2 ms. The space-time plot of the pressure is from the simulation results on the axis of symmetry of the tube.

The dynamics of the transient behavior is now examined in more detail using Fig. 7a and Fig. 8. At approximately $t = -0.6$ ms (event 1), the projectile impacts on the buffer. This pushes the buffer down and generates a pressure wave within the liquid as described above. This pressure wave, the first incident wave, propagates downward into the liquid at the Korteweg speed of 1350 m/s (i.e., parallel to the characteristic lines shown in Fig. 7a). When the wave reaches the bottom of the tube at approximately $t = 0$ ms (event 2), reflection produces a wave traveling upward which will be called the first reflected wave.

The hoop strains associated with the first incident and reflected pressure waves are approximately 300 $\mu\varepsilon$, except close to the bottom wall where the hoop strains are close to 600 $\mu\varepsilon$ due to the pressure increase associated with reflection.

When the first reflected wave reaches the bottom end of the buffer, it reflects (event 3) producing the second incident wave traveling downward into the liquid. This wave, however, is *immediately* followed by a tension wave due to the motion of the buffer. This is because upon reflection of the first reflected wave on the buffer (event 3), the liquid pressure below the buffer is large. The resulting force applied on the buffer accelerates the latter upward, and this upward motion produces a tension wave just behind the second incident wave. This tension also explains why the second reflected wave (the one produced during event 4) is eventually annihilated (event 5).

Regarding the axial strains, assuming zero axial stress[2] and using shell theory yields $\varepsilon_z = -\nu\varepsilon_\theta$ [16]. This implies the axial strains are produced through the Poisson effect. Using the experimental results it is possible to verify that the relation above is approximately satisfied; the magnitude of the axial strains is approximately one-third that of the hoop strains.

Case 2

Case 2 has the same geometry and impact speed as case 1 but has a "small", 3.5 mm, air gap between the bottom of the buffer and the water surface. The air gap drastically affects both the interaction of the projectile and buffer as well as the transmission of pressure waves into the liquid column.

Pressures P1 and P2 are shown in Fig. 10. Again, both signals are very similar in trend and magnitude. The pressure history is however more complicated than it was in case 1; there are now multiple pressure peaks. The measured peak pressure is approximately 11.0 MPa; 30% lower than the peak pressure measured for case 1. This is because the water column is now pressurized through the isentropic compression of the air gap. LS-DYNA does not predict all the fine details of the experimental pressure traces, but it does predict the presence of multiple pressure peaks.

The motion of the projectile and the buffer along with a space-time plot of the pressure is shown in Fig. 9. The projectile bounces off the buffer resulting in multiple impacts between the projectile and the buffer, which is different from case 1 where only one impact was observed. When there is an air gap, the projectile, the buffer and the air gap now form a spring-mass system, and the air gap is equivalent to a non-linear spring. Although it is not discussed in this paper, using rigid body mechanics (i.e., conservation of momentum and energy) with a non-linear spring for the air gap enables reasonable quantitative predictions of the interactions between the projectile, the buffer and the air gap.

It is possible to approximate the pressure within the air gap as uniform since the transit time of the wave is short; the waves within the air gap can achieve multiple reverberations during the compression or the relaxation of the gap. In fact, the transit time of the waves within the air gap is at most 10 μs for case 2.

As previously mentioned, there are now 3 distinguishable impacts between the projectile and the buffer (events 1, 3 and

[2] This assumption is only valid close to the top end of the tube.

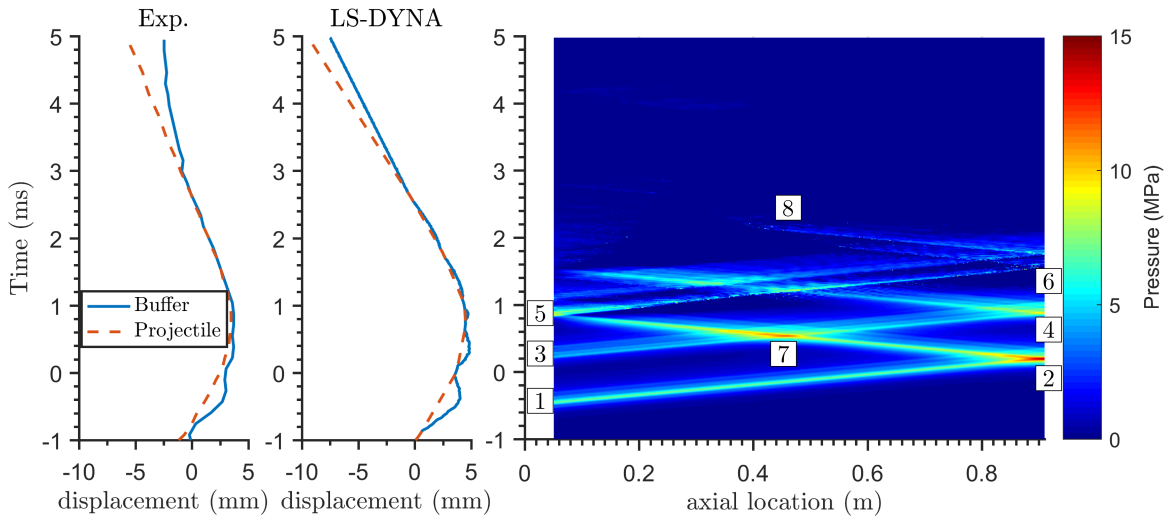

FIGURE 9: MOTION OF THE BUFFER AND THE PROJECTILE WITH A SPACE-TIME PRESSURE PLOT (CASE 2).

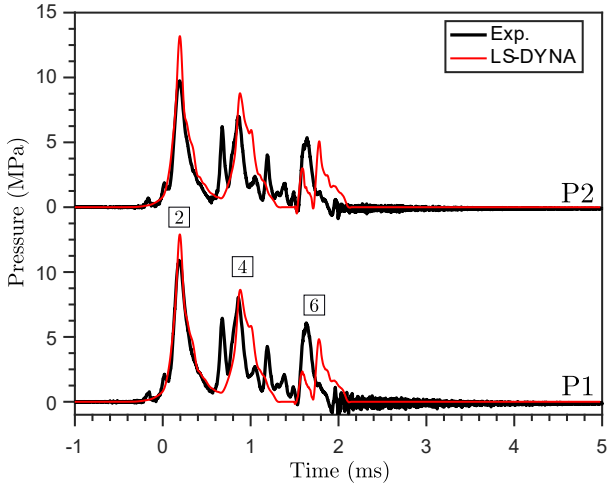

FIGURE 10: PRESSURE AT THE BOTTOM END (CASE 2).

5), each of which results in the production of a pressure wave. Each of these waves will reflect at the bottom wall (events 2, 4 and 6) and propagate upward, toward the buffer. However, only the wave due to the first impact has enough time to reach the top of the liquid column. This is because the reflection of the first compression wave (event 5) happens at a free surface and this produces a tension wave. This can be understood using Eq. 1: medium 1 is water and medium 2 is air. The acoustic impedance of air is much smaller than the acoustic impedance of water. Therefore, $\Delta P_r \approx -\Delta P_i$: the sign of the pressure wave changes, and a compression wave becomes a tension wave upon reflection.

As in case 1, the buffer starts moving upward after reflection (event 5) occurs, and this creates an expansion wave which leads to tension in the liquid. Eventually, all this tension produced at the top end of the tube will propagate throughout the tube and interfere destructively with the second and third waves before they reach the buffer. At t = 2.5 ms (event 8), the entire water column is under tension and cavitation occurs, probably distributed throughout the column as observed by Inaba and Shepherd [10].

Another interesting feature is the possibility of having some constructive interference between the multiple waves propagating within the tube. This is observed at event 7 where the incident wave due to the second impact interacts constructively with the reflected wave due to the first impact. Although the strains are not shown, this constructive interference also increases the hoop and axial strains locally and instantaneously. This means that the peak pressure within the tube does not necessarily occur at the bottom wall.

Case 3

Case 3 is identical to case 2 except there is initially a "large", 12.0 mm, air gap between the buffer and the water surface. The size of the air gap drastically affects the timing of the multiple impacts between the projectile and the buffer.

Pressures P1 and P2 are shown in Fig. 11. The two pressure traces are again very close in trend and magnitude. The match between the experiment and the simulation is also good. It is now possible to distinguish two main pressure waves. The first one reaches a peak pressure of approximately 3.9 MPa at t = 0.3 ms, and the pressurization happens very slowly; the pressure takes $\sim$ 1 ms to reach its peak value. The second pressure wave is very sharp and reaches a peak value of 7.2 MPa at t = 1.75 ms.

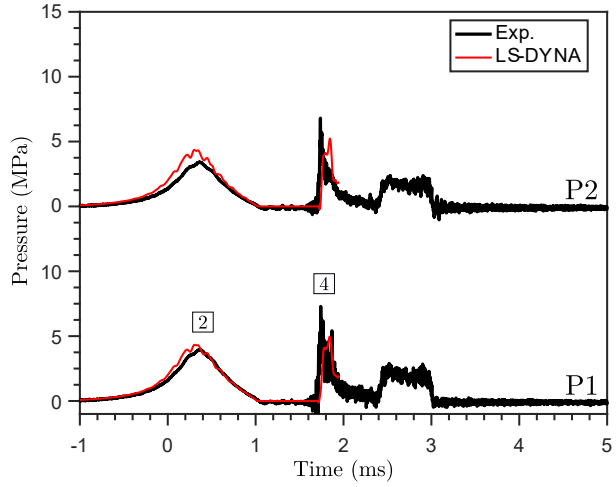

FIGURE 11: PRESSURE AT THE BOTTOM END (CASE 3).

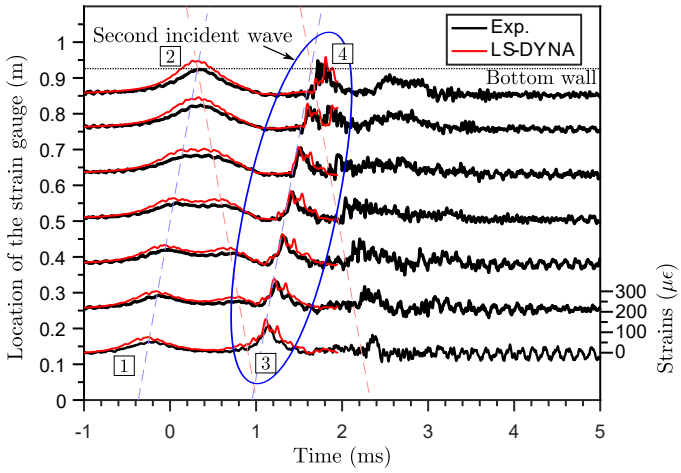

FIGURE 12: HOOP STRAINS (CASE 3).

The rise time associated with this pressure wave is approximately 30 μs. Between the first and the second pressure waves (t between 1.0 and 1.6 ms), the liquid is under tension and cavitation occurs. Unlike case 1, the second pressure wave is *not* due to the reflection of the first pressure wave.

The projectile and buffer's motion along with a space-time plot of the pressure are shown in Fig. 13. There are multiple impacts between the projectile and the buffer. The first one (event 1) produces the very slow pressurization of the water column through compression of the air gap. This corresponds to the first pressure wave visible on both P1 and P2. When this first wave reflects off the bottom wall (event 2), a compression wave traveling upward is produced. When this wave reaches the top of the tube

TABLE 3: RISE TIMES OF THE SECOND INCIDENT WAVE.

Station	S1	S2	S3	S4	S5	S6	S7	P1	P2
T (μs)	360	170	160	130	70	70	50	30	30

and reflects off the free surface between the air and the liquid, it becomes a tension wave for the same reasons as in case 2 and results in distributed cavitation. This tension wave is followed by the second incident wave, which is produced by the second impact of the projectile on the buffer (event 3). This second incident wave is propagating into a cavitating liquid.

The effective sound speed in a cavitating liquid (i.e., a two phase mixture) is a strong function of the vapor fraction [17]. The collapse of the cavities under pressure will increase the wave speed and produce wave steepening. This results in the second incident pressure wave becoming a shock wave before reaching the bottom end of the tube. This explains the very short rise time of the second pressure wave (see Tab. 3).

The steepening of the second pressure wave is also observed on the hoop strains shown in Fig. 12. For stations S3 to S7, careful reading of the plot shows that the second incident wave is preceded by a negative hoop strain. Visually, the steepening of the wave is observed between locations S3 to S7. Quantitatively, the rise times of the hoop strains and pressures associated with the second incident wave are summarized in Tab. 3.

LS-DYNA simulates the steepening of the pressure wave despite the absence of an explicit cavitation model. As mentioned before, this is because of the boundary condition between the aluminum tube and the water which mimics the effect of cavitation. We confirmed that using a boundary condition which allows for tensile forces between the two surfaces eliminates the steepening of the wave.

Case 4

Case 4 is identical to case 3 except there is a converging section. The dynamics are identical; only the pressure at the bottom of the test specimen differs between theses cases.

Both P1 and P2 are shown in Fig. 14. As in case 3 there are two main pressure waves produced by the impacts between the projectile and the buffer. We first consider the first wave which has a slow rise time of order $\sim$ 1 ms. The peak pressure is approximately 4.3 MPa and is very well predicted by LS-DYNA. More importantly, the peak pressure is the same above and at the end of the converging section; there is no amplification of the pressure due to the converging section.

For the second pressure wave, the rise time is approximately 16 μs (measured using P2). The peak pressure measured at the

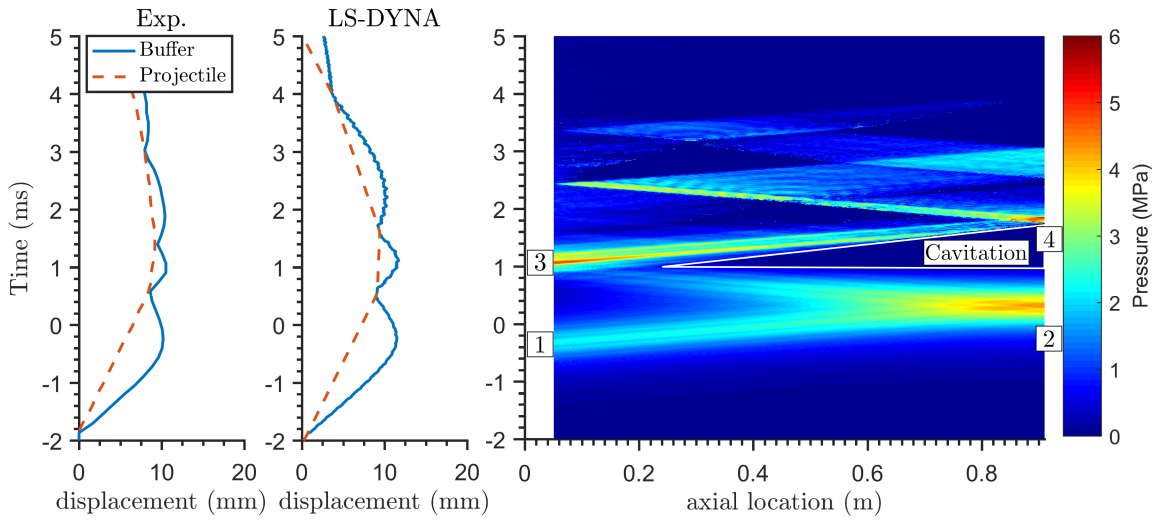

FIGURE 13: MOTION OF THE BUFFER AND THE PROJECTILE WITH A SPACE-TIME PRESSURE PLOT (CASE 3).

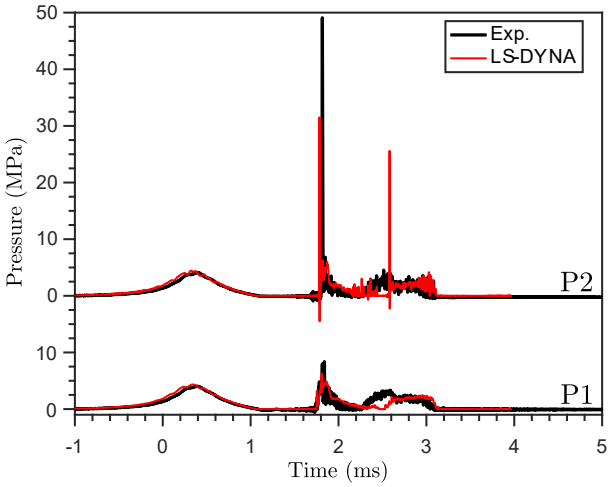

FIGURE 14: PRESSURE AT THE BOTTOM END (CASE 4).

apex of the converging section (P2) is approximately 50 MPa, and the peak pressure measured above the converging section (P1) is about 8.4 MPa; the pressure was amplified by a factor of six in the converging section.

To explain the results above, we examine the transit time of the pressure waves for a round trip within the converging section. Assuming the cone remains filled with pure liquid, the time scale representing the transit of the acoustic waves in the cone is $2l/a$ where l is the length of the converging section. With the present geometry, this transit time is $\sim 24\ \mu$s.

Because the first pressure wave has a rise time which is much longer than the transit time of the wave through the converging section, there is no amplification of the pressure wave within the converging section. The pressurization of the cone happens slowly, and the pressure has time to equilibrate throughout the cone during the pressurization.

On the contrary, the rise time associated with the second pressure wave is of the same order as the transit time. The pressure is not uniform throughout the cone and amplification of the pressure is possible. As discussed in case 3, the very short rise time of the second pressure is attributed to wave steepening associated with cavitation.

A numerical simulation has been performed with a refined grid (by a factor of 4). The pressure inside the cone at the arrival of the second, sharp pressure wave is shown in Fig. 15 at different times. Pressures in excess of 5 MPa are represented in magenta, and the motion of the wave front is indicated with black arrows.

At $t = 1.764$ ms, the wave front enters the converging section. At $t = 1.770$ ms, a part of the wave has been transmitted into the cone, and a part of the wave has been reflected. The transmitted wave inside the cone is also converging toward the axis of symmetry. At $t = 1.776$ ms and $t = 1.778$ ms, the pressure is amplified as the wave converges toward the axis of symmetry. This focusing of the wave onto the axis of symmetry is responsible for the amplification of the sharp pressure waves.

CONCLUSION

The impulsively-generated pressure and strain transients inside a cylindrical, fluid-filled tube were studied experimentally and numerically. The effect of an air gap and a converging section were studied using four cases.

Case 1, the simplest case, has no air gap and no converging section. It was found that the upward motion of the buffer upon

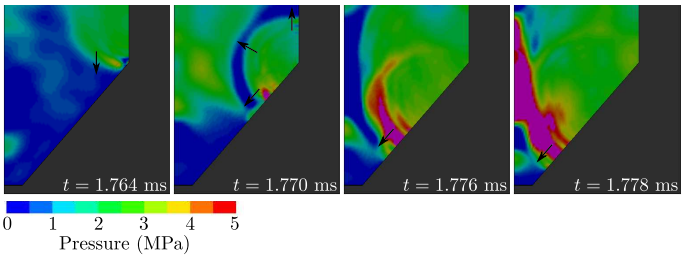

FIGURE 15: PRESSURE IN THE CONE (CASE 4).

reflection of the pressure wave on the buffer produces a tension wave, and this tension results in distributed cavitation.

Case 2 has the same geometry as case 1 but a small air gap was introduced between the buffer and the water. The presence of an air gap drastically affects the dynamics of the projectile-buffer; there are now multiple collisions between the projectile and the buffer resulting in multiple pressure waves within the tube. Constructive interference between the waves is observed.

Case 3 is identical to case 2 except the air gap is large. The size of the air gap drastically affects the timing of the multiple impacts between the projectile and the buffer. As a result, the wave generated through the second impact propagates in a cavitating liquid, and wave steepening leading to shock waves is observed.

Case 4 is identical to case 3, except there is a converging section at the bottom end of the tube. The converging section amplifies substantially the sharp pressure wave resulting from wave steepening. This amplification of the wave is due to the convergence of the pressure wave toward the axis of symmetry of the tube.

The results suggest that combining an air gap and a converging section can produce very large pressures and stresses in the cone area of a syringe geometry. In the case of a glass syringe used in autoinjectors, the resulting stresses may lead to failure of the device. In the future, the effect of the translational motion of the syringe on the pressure transients will be studied experimentally and numerically.

ACKNOWLEDGMENT

This work is sponsored by Amgen through the Caltech-Amgen Research Collaboration Agreement for Chem-Bio-Engineering Awards.

REFERENCES

[1] Limmroth, V., and Gerbershagen, K., 2014. "Single-use autoinjector for once-weekly intramuscular injection of ifn-1a.". *Expert Opinion on Drug Delivery,* ***11***(12), p. 1969.

[2] Schiff, M., Jaffe, J., Freundlich, B., and Madsen, P., 2014. "New autoinjector technology for the delivery of subcutaneous methotrexate in the treatment of rheumatoid arthritis.". *Expert Review of Medical Devices,* ***11***(5), p. 447.

[3] Rathore, N., Shah, M., and Kolhe, P., 2013. *Sterile Product Development. [electronic resource] : Formulation, Process, Quality and Regulatory Considerations.* AAPS Advances in the Pharmaceutical Sciences Series: 6. New York, NY : Springer New York : Imprint: Springer, 2013.

[4] Lange, J., and Thompson, I., 2013. "Self-Injection Devices". In *Encyclopedia of Pharmaceutical Science and Technology*, 4^{th} ed. Taylor & Francis, pp. 3132–3143.

[5] Akers, M. J., 2010. *Sterile Drug Products: Formulation, Packaging, Manufacturing and Quality*. CRC Press.

[6] Fry, A., 2014. Injecting Highly Viscous Drugs. On the WWW. `http://www.pharmtech.com/`.

[7] Wiggert, D. C., 2001. "Fluid transients and fluid-structure interaction in flexible liquid-filled piping.". *Applied Mechanics Reviews,* ***54***(5), p. 455.

[8] Wylie, E. B., Suo, L., and Streeter, V. L., 1993. *Fluid transients in systems.* Englewood Cliffs, NJ : Prentice Hall.

[9] Watters, G. Z., 1984. *Analysis and control of unsteady flow in pipelines.* Boston : Butterworths.

[10] Inaba, K., and Shepherd, J. E., 2010. "Dynamics of Cavitating Flow and Flexural Waves in Fluid-Filled Tubes Subject to Axial Impact". In Proceedings of the ASME 2010 Pressure Vessels & Piping Division. Paper PVP2010-25989.

[11] Shepherd, J. E., and Inaba, K., 2010. "Shock Loading and Failure of Fluid-Filled Tubular Structures". In *Dynamic Failure of Materials and Structures*, G. Ravichandran and Y. Rajapakse, eds. Springer, pp. 153–190.

[12] J. O. Hallquist, 2016. *LS-DYNA : THEORY MANUAL*, latest ed. Livermore Software Technology Corporation, Livermore, California (USA). `http://www.lstc.com`.

[13] Wu, Z., Zong, Z., and Sun, L., 2014. "A Mie-Grüneisen mixture Eulerian model for underwater explosion.". *Engineering Computations,* ***31***(3), p. 425.

[14] Kojima, T., Inaba, K., Takahashi, K., Triawan, F., and Kishimoto, K. "Dynamics of Wave Propagation Across Solid-Fluid Movable Interface in Fluid-Structure Interaction". *Journal of Pressure Vessel Technology,* ***139***(3), pp. 031308–031308–9.

[15] Liepmann, H. W., and Roshko, A., 2001. *Elements of gasdynamics.* Mineola, N.Y. : Dover Publications, 2001.

[16] Bitter, N. P., and Shepherd, J. E., 2013. "On the Adequacy of Shell Models for Predicting Stresses and Strains in Thick-Walled Tubes Subjected to Detonation Loading". In Proceedings of the ASME 2013 Pressure Vessels & Piping Division. Paper PVP2013-97148.

[17] Brennen, C. E., 2014. *Cavitation and bubble dynamics.* New York : Cambridge University Press, 2014.